Research Square

Preprints are preliminary reports that have not undergone peer review.
They should not be considered conclusive, used to inform clinical practice,
or referenced by the media as validated information.

Data-Driven EEG Band Boundaries Converge Near Euler's Number: A Multi-Method Analysis Across 244 Subjects

andrei ursachi

contact@andreiursachi.eu

Independent https://orcid.org/0009-0002-6114-5011

Research Article

Keywords: EEG, frequency band boundaries, data-driven, self-similarity, Euler's number, golden ratio, spectral parameterization, multi-method comparison

Posted Date: February 26th, 2026

DOI: https://doi.org/10.21203/rs.3.rs-8935579/v1

License: This work is licensed under a Creative Commons Attribution 4.0 International License.
Read Full License

Additional Declarations: The authors declare no competing interests.

Abstract

Conventional EEG frequency band boundaries (e.g., theta 4–8 Hz, alpha 8–13 Hz) were established by visual inspection decades ago and have never been systematically tested against mathematical organizing principles. We applied three independent boundary detection methods—spectral parameterization (FOOOF/specparam), spectral derivative analysis, and cross-frequency topographic correlation—to resting-state EEG from N = 244 subjects across three public datasets. All three methods placed the alpha–beta to theta–alpha boundary ratio nearest to e − 1 = 1.718 among the tested constants (φ, e − 1, 2:1, √2): FOOOF 1.853 ± 0.045 (N = 55), derivative 1.826 ± 0.039 (N = 158), correlation 1.685 ± 0.031 (N = 171, TOST-equivalent at ε = 0.10). A mixed-effects model yielded a population-level intercept of 1.787 (95% CI: 1.717–1.857), with e − 1 falling within the confidence interval. Permutation testing confirmed this clustering as non-random ($p < 0.002$). The boundary ratio was statistically equivalent to the spectral centroid ratio from our companion paper (paired t: $p = 0.35$, Cohen's $d = 0.075$, TOST-equivalent at ε = 0.15), confirming self-similar organization across spectral description levels. Empirical boundaries diverged substantially from convention: the beta–gamma boundary averaged 25.3 Hz (vs. conventional 30 Hz), while the theta–alpha boundary (7.73 Hz) was consistent with Klimesch's (2013) theoretical prediction of 7.5 Hz. Power analysis revealed that studies with $N < 30$ systematically favor φ, while adequately powered samples converge toward e − 1—suggesting that some published reports of golden-ratio organization may reflect insufficient statistical power.

1. Introduction

The division of the human electroencephalogram (EEG) into canonical frequency bands—delta (0.5–4 Hz), theta (4–8 Hz), alpha (8–13 Hz), beta (13–30 Hz), and gamma (30–45 Hz)—is among the most fundamental conventions in neuroscience. These boundaries, established through visual inspection of spectral plots in the mid-twentieth century, underpin thousands of studies linking band-specific power to cognition, pathology, and pharmacology. Yet the boundaries themselves have received remarkably little empirical scrutiny.

Three mathematical frameworks have been proposed for the *spacing* of oscillatory bands, though all address center frequencies rather than boundaries. Penttonen and Buzsáki (2003) demonstrated that center frequencies form a geometric progression with ratio approximately $e \approx 2.718$ on a natural logarithmic scale, conserved across mammalian species. Pletzer, Kerschbaum, and Klimesch (2010) showed that adjacent sub-band center frequencies relate by the golden ratio $\varphi \approx 1.618$, which, as the most irrational number, produces maximal desynchronization between co-active oscillators—a prediction grounded in the Kolmogorov–Arnold–Moser (KAM) theorem. Van Albada, Kerr, Chiang, Rennie, and Robinson (2013) reconciled these frameworks by noting that $\varphi^2 \approx 2.618 \approx e$, meaning two golden-ratio steps approximately equal one natural-logarithmic step.

Klimesch (2013) provided the only theoretical derivation of band *boundaries*, proposing a "golden mean rule" in which boundaries are placed at frequencies maximally separated from adjacent center

frequencies. However, these predictions have never been empirically tested using data-driven methods. In our companion papers (Ursachi, 2026a, in production; Ursachi, 2026b, under review), we demonstrated that spectral centroid ratios across N = 244 subjects cluster near 1.778 within a corrugated constraint landscape exhibiting alternating exponential–harmonic organization.

Here we ask: do the *boundaries* between frequency bands exhibit the same mathematical organization as the *centroids* within bands? If so, EEG frequency architecture would be self-similar—the same scaling tendency recurring at multiple levels of spectral description. We apply three independent boundary detection methods to the same three public datasets, test boundary ratios against four mathematical constants, and evaluate whether conventional boundaries approximate these predictions.

2. Materials and Methods

2.1 Datasets

Three publicly available resting-state EEG datasets were analyzed, identical to those in the companion papers. (1) PhysioNet EEG Motor Movement/Imagery (EEGBCI): N = 109 subjects, 64-channel, 160 Hz sampling rate, eyes-closed baseline (Goldberger et al., 2000; Schalk et al., 2004). (2) OpenNeuro ds003969: N = 98 subjects, 64-channel BrainVision format, resampled to 256 Hz, eyes-closed resting state. (3) Zenodo Alpha Waves: N = 37 subjects, 16-channel, 512 Hz, eyes-closed resting state (Rodrigues et al., 2017). Total N = 244.

2.2 Spectral estimation

Power spectral density (PSD) was computed using Welch's method (4-second Hanning windows, 50% overlap) for each channel, then averaged across channels over 1–45 Hz. For ds003969, raw BDF files were resampled to 256 Hz immediately after loading to manage memory constraints, then re-referenced to average. All processing used MNE-Python (Gramfort et al., 2013).

2.3 Boundary detection methods

2.3.1 Method A: Spectral parameterization (FOOOF)

The specparam algorithm (Donoghue et al., 2020) was applied to channel-averaged PSDs over 1–45 Hz, decomposing the spectrum into aperiodic (1/f) and periodic (Gaussian peaks) components. Boundaries were defined as midpoints between adjacent peak centers. Quality filtering required $R^2 > 0.90$ and at least three periodic peaks. Sensitivity analyses using R^2 thresholds of 0.80, 0.85, 0.90, 0.95, and 0.97 confirmed that boundary ratios remained stable across quality criteria (Section 3.12).

2.3.2 Method B: Spectral derivative analysis

The aperiodic component was subtracted from the raw PSD to isolate periodic activity. The periodic-only spectrum was smoothed using a Savitzky–Golay filter (window length = 11, polynomial order = 3). First-derivative zero-crossings identified spectral peaks; local minima between adjacent peaks defined

boundaries. Boundaries were assigned to δ–θ, θ–α, α–β, and β–γ transitions based on frequency position.

2.3.3 Method C: Cross-frequency topographic correlation

Inspired by Cohen (2021), this method exploits multichannel spatial information. For each frequency bin (0.5 Hz resolution), the power topography across all channels was computed. A frequency-by-frequency correlation matrix was constructed; hierarchical clustering identified groups of frequencies sharing similar spatial distributions; boundaries were defined as cluster transitions.

2.4 Boundary ratio computation

For each subject with at least two detected boundaries, the ratio αβ/θα (alpha–beta boundary divided by theta–alpha boundary) served as the primary outcome.

2.5 Statistical analysis

Boundary ratios were tested against four mathematical constants: φ = 1.618, e − 1 = 1.718, 2:1 = 2.000, and √2 = 1.414. For each, one-sample t-tests assessed difference; two one-sided tests (TOST) assessed equivalence at ε = 0.10 and 0.15. AIC compared constant-based models.

2.6 Mixed-effects modeling

To account for clustering by dataset and method, a linear mixed-effects model was fit: boundary ratio ~ method + (1 | dataset), with method as a fixed effect and dataset as a random intercept. The population-level intercept was compared against each mathematical constant. Between-dataset variance and intraclass correlation coefficient (ICC) were reported.

2.7 Permutation testing

To evaluate whether observed clustering near specific constants was non-random, null distributions were generated by uniformly sampling boundary frequencies within physiologically plausible ranges (2–40 Hz), computing ratios, and repeating 10,000 times per method. The proportion of null ratios falling within ± 0.10 of the empirical mean provided the permutation p-value.

2.8 Self-similarity testing

For subjects with both centroid ratios (from companion Paper 2) and boundary ratios, a paired t-test and TOST equivalence test (ε = 0.05, 0.10, 0.15) compared the two levels of spectral description. Cohen's d quantified effect size.

2.9 Power analysis

To examine the effect of sample size on constant identification, subsamples of N = 10, 20, 30, 50, 75, 100, and 150 were drawn 1,000 times from the correlation method data. For each subsample, the nearest constant was recorded, generating a proportion curve across sample sizes.

3. Results

3.1 Sample sizes

After quality filtering, the derivative method provided the largest sample (N = 158 for αβ/θα ratios), followed by correlation (N = 171) and FOOOF (N = 55). EEGBCI contributed the majority of FOOOF boundaries; ds003969 and Alpha Waves contributed primarily through derivative and correlation methods (Table 1).

Table 1
Sample sizes for boundary ratios (αβ/θα) by method and dataset.

Dataset	Total N	FOOOF	Derivative	Correlation
EEGBCI	109	46	83	88
DS003969	98	9	51	50
Alpha Waves	37	0	24	33
Total	244	55	158	171

3.2 Empirical boundary frequencies

Data-driven boundaries diverged from conventional definitions (Figs. 1–2). The derivative method yielded: δ–θ = 4.27 ± 0.73 Hz (conventional: 4.0; $p < 0.001$), θ–α = 7.73 ± 1.29 Hz (conventional: 8.0; $p = 0.021$; not significantly different from Klimesch's prediction of 7.5 Hz, $p = 0.056$), α–β = 13.50 ± 1.97 Hz (between conventional 13.0 and Klimesch's 14.0; $p < 0.002$ for both), and β–γ = 25.26 ± 4.82 Hz ($t = -12.40$, $p < 0.001$ vs. conventional 30 Hz; $t = -7.17$, $p < 0.001$ vs. Klimesch's 28 Hz). The beta–gamma boundary deviation (− 5 Hz) has direct implications for studies defining beta as 13–30 Hz.

3.3 Boundary ratios: nearest to e − 1 across methods

The primary outcome—the ratio αβ/θα—was nearest to e − 1 = 1.718 for all three methods among the tested constants (Table 2, Fig. 3). FOOOF yielded 1.853 ± 0.045 (N = 55), derivative 1.826 ± 0.039 (N = 158), and correlation 1.685 ± 0.031 (N = 171). The correlation method was TOST-equivalent to e − 1 at $\varepsilon = 0.10$. FOOOF and derivative were significantly different from e − 1 ($p = 0.005$ and $p = 0.006$, respectively), with estimates slightly above 1.718. All methods rejected φ, √2, and (except FOOOF marginally) 2:1. AIC selected e − 1 for correlation; the empirical mean outperformed all constants for FOOOF and derivative, consistent with the companion paper's finding that no single constant fully captures individual-level variation.

Table 2
Boundary ratios (αβ/θα) by method.

Method	N	Ratio ± SE	Nearest	p vs φ	p vs e − 1	p vs 2:1
FOOOF	55	1.853 ± .045	e − 1	< .001	.005	.021
Derivative	158	1.826 ± .039	e − 1	< .001	.006	< .001
Correlation	171	1.685 ± .031	e − 1	.031	.288	< .001

3.4 Mixed-effects model

A linear mixed-effects model with method as fixed effect and dataset as random intercept yielded a population-level intercept of 1.787 ± 0.036 (95% CI: 1.717–1.857). The value e − 1 = 1.718 falls within this confidence interval. Between-dataset variance was minimal (ICC = 0.001), indicating that dataset identity contributed negligibly to ratio variation after accounting for method. Method was a significant predictor (p = 0.003), confirming that detection approach—not recording setup—drives systematic differences in boundary ratios.

3.5 Permutation testing

Permutation null distributions constructed from randomly placed boundaries showed that the empirical clustering near 1.7–1.9 was unlikely to arise by chance (p < 0.002 for all three methods; Fig. 14). This confirms that boundary ratios reflect genuine spectral organization rather than an artifact of ratio computation over arbitrary frequency ranges.

3.6 Self-similarity: centroids ≈ boundaries

For N = 158 subjects with both centroid and boundary measures, the spectral centroid ratio α/θ averaged 1.788 ± 0.103 and the boundary ratio αβ/θα averaged 1.826 ± 0.485. A paired t-test found no significant difference (p = 0.35). TOST confirmed equivalence at ε = 0.15 (Cohen's d = 0.075). Both ratios are nearest to e − 1, and the group-level difference of 0.038 is negligible (Fig. 4). This confirms that the same scaling tendency governs spectral structure at two distinct levels: within-band centroids and between-band boundaries.

Within-subject correlation was non-significant (r = − 0.106, p = 0.185; Fig. 6), indicating that self-similarity is a population-level architectural property rather than an individual trait. This dissociation may reflect distinct neural mechanisms governing oscillatory peak frequencies (centroids) versus the spectral regions of inter-regime transition (boundaries).

3.7 Conventional boundary ratio 13/8 ≈ φ

It is noteworthy that the conventional boundary ratio 13/8 = 1.625 differs from φ = 1.618 by only 0.007 (0.4%). This proximity connects to Pletzer et al.'s (2010) KAM analysis: boundaries placed at golden-ratio spacing maximize desynchronization stability. Whether early EEG researchers converged on φ-like

boundaries through careful spectral observation or coincidence cannot be determined, but the close approximation is striking. Data-driven analysis shifts the estimate from this φ-like conventional value toward the e − 1 region.

3.8 Dataset replication

Boundary ratios showed dataset-specific variation using the derivative method (Fig. 8, Fig. 13): EEGBCI 1.750 ± 0.049 (N = 83, nearest e − 1, p = 0.52), ds003969 1.869 ± 0.069 (N = 51, nearest 2:1, p = 0.07), Alpha Waves 1.997 ± 0.108 (N = 24, nearest 2:1, p = 0.98). All datasets were non-significant versus their nearest constant. The between-dataset effect size was moderate (EEGBCI vs. ds003969: d = − 0.42, p = 0.024). However, the mixed-effects model (Section 3.4) showed that dataset clustering was minimal (ICC = 0.001), suggesting that this variation reflects method–dataset interactions rather than fundamental population differences.

3.9 Cross-method agreement

Methods agreed moderately for the theta–alpha boundary (FOOOF–derivative: r = 0.508, p < 0.001, N = 47; mean difference 0.70 Hz) but poorly for the alpha–beta boundary (all pairwise r < 0.12, p > 0.27; Fig. 5). This dissociation indicates that the three methods detect partially distinct spectral features, yet converge on similar boundary ratios. The ratio metric proves more robust than absolute boundary position, consistent with scale-free spectral organization.

3.10 Aperiodic slope

Aperiodic slope showed no relationship to any boundary frequency or ratio (all |r| < 0.04, p > 0.67, N = 158; Fig. 7). Boundary placement is determined by periodic structure, not the 1/f background.

3.11 FOOOF selection bias analysis

Subjects with usable FOOOF boundaries (N = 55) differed from those without (N = 189) in model fit (R^2: p < 0.001) and number of detected peaks (p < 0.001), as expected given the quality filter. Crucially, aperiodic spectral slope did not differ (p = 0.13), indicating no systematic bias in the underlying spectral shape of included versus excluded subjects. Dataset composition differed significantly (χ^2 p < 0.001), with EEGBCI overrepresented, reflecting that 64-channel, lower-sampling-rate recordings yield more discrete spectral peaks amenable to FOOOF decomposition.

3.12 FOOOF sensitivity analysis

Boundary ratios remained stable across quality thresholds: R^2 > 0.80 (1.867, N = 79), R^2 > 0.85 (1.856, N = 67), R^2 > 0.90 (1.853, N = 55), R^2 > 0.95 (1.849, N = 38), R^2 > 0.97 (1.851, N = 24). The maximum variation across thresholds was 0.018, confirming that boundary ratio estimates are insensitive to quality filter stringency (Fig. 16).

3.13 Power analysis: sample size and constant identification

Subsampling analysis of the correlation method data revealed a systematic shift in “nearest constant” as a function of sample size (Fig. 15). At $N < 30$, the golden ratio φ was identified as the nearest constant in the majority of subsamples. At $N \geq 30$, $e - 1$ overtook φ as the modal nearest constant. This pattern suggests that published reports of golden-ratio organization in EEG may partially reflect insufficient statistical power: the group mean shifts from the vicinity of φ toward $e - 1$ as estimation precision improves with larger samples.

4. Discussion

4.1 Population-level scaling near e − 1

The principal finding is that data-driven boundary ratios cluster nearest to $e - 1 = 1.718$ among the tested constants, with a mixed-effects population intercept of 1.787 (CI: 1.717–1.857). We emphasize that this represents a population-level scaling tendency rather than a precise mathematical identity: individual boundary ratios are broadly distributed (SD ≈ 0.4), and both FOOOF and derivative method means exceed 1.718 by approximately 0.1–0.15 units. The claim is not that boundaries are fixed at $e - 1$, but that $e - 1$ provides the best single-constant approximation for the population mean among the theoretically motivated candidates tested.

This convergence was not apparent in preliminary analyses with smaller samples: with $N = 102$, the correlation method appeared to favor $\varphi = 1.618$; expansion to $N = 171$ revealed that the population estimate lies nearer to $e - 1$. Power analysis confirmed that this shift is systematic: underpowered studies ($N < 30$) preferentially identify φ. This finding has implications beyond the present study, suggesting caution in interpreting constant-identification claims from small-sample spectral analyses.

4.2 Self-similar spectral architecture

The near-identity between centroid ratios (1.788) and boundary ratios (1.826)—confirmed by equivalence testing ($d = 0.075$)—demonstrates self-similar spectral architecture across two levels of description. This property was suggested theoretically by Klimesch (2013, 2018) but never tested empirically. The architecture parallels scale-free organization in other biological systems, where the same mathematical relationships recur across levels of spatial or temporal description.

The lack of within-subject correlation ($r = -0.106$) indicates that self-similarity is an emergent population-level property. Individual subjects may have centroid ratios near φ but boundary ratios near 2:1; only the population means converge near $e - 1$ at both levels. This dissociation may reflect distinct neural generators governing peak frequencies versus regime transitions.

4.3 Klimesch’s predictions: partial validation

Our data partially validate Klimesch's (2013) boundary predictions. The theta–alpha boundary (empirical: 7.73 Hz) was not significantly different from Klimesch's predicted 7.5 Hz ($p = 0.056$), providing the first empirical support for his golden mean rule at this transition. However, the beta–gamma boundary (25.3 Hz) fell below both Klimesch's prediction (28 Hz) and convention (30 Hz). Overall, Klimesch's framework provides a useful first approximation for the theta–alpha transition but overestimates higher-frequency boundaries.

4.4 The beta–gamma boundary: a 5 Hz discrepancy

The empirical beta–gamma boundary averaging 25.3 Hz—nearly 5 Hz below the conventional 30 Hz cutoff—is perhaps the most practically significant finding. Activity between 25 and 30 Hz, conventionally classified as beta, may be better characterized as transitional or low-gamma. Given that beta oscillations are central to research on motor planning, attention, Parkinson's disease, and anxiety, a systematic misspecification of the upper beta boundary could affect both power estimates and functional interpretations. We recommend that researchers consider data-driven boundary definitions or, at minimum, report results for both the conventional 13–30 Hz and the empirically supported 13–25 Hz beta range.

4.5 The hidden φ in conventional boundaries

It is noteworthy that the conventional ratio $13/8 = 1.625$ approximates $\varphi = 1.618$ within 0.4%. This observation connects to the KAM theorem analysis of Pletzer et al. (2010): boundaries at golden-ratio spacing maximize desynchronization stability. Our data-driven analysis shifts the estimate from this conventional φ-like value toward the $e - 1$ region, suggesting that modern multi-method analysis reveals a different facet of spectral organization than visual inspection captured.

4.6 Method dependence and the robustness of ratios

The three detection methods agreed on the nearest constant ($e - 1$) but disagreed on absolute boundary positions, with systematic offsets reflecting different spectral features targeted by each method. FOOOF places boundaries at periodic peak troughs; derivative analysis identifies spectral inflection points; correlation analysis detects topographic transitions. That boundary ratios converge despite absolute frequency disagreement suggests that the ratio is the more fundamental quantity—consistent with the scale-free properties expected of fractal spectral organization.

4.7 Null findings

Several hypothesized relationships were not supported. Aperiodic spectral slope showed no relationship to boundary placement. Angular velocity analysis (boundary frequency differences) provided no additional organizing principle beyond boundary ratios, as the two measures shared over 77% of variance (Supplementary Material). Fibonacci-like accumulation of boundary differences held in fewer than half of subjects. Within-subject centroid–boundary correlation was non-significant. These null results narrow the space of viable models for band boundary organization.

4.8 Limitations

Several limitations should be noted. First, FOOOF yielded usable ratios for only 55 subjects (22.5%), though selection bias analysis confirmed no systematic spectral shape difference between included and excluded subjects. Second, dataset-specific variation was present (range: 1.750–1.997), though the mixed-effects ICC (0.001) indicates this reflects method–dataset interactions rather than population-level heterogeneity. Third, the constant-identification framework tested four pre-selected constants; a broader search might identify closer approximations, though permutation testing confirmed that clustering near the empirical mean was non-random. Fourth, analysis was limited to resting-state, eyes-closed conditions; boundaries during tasks or altered states may differ. Fifth, the self-similarity claim rests on group-level equivalence without within-subject coupling.

4.9 Future directions

Preregistered replication with larger datasets (e.g., the MPI Leipzig LEMON dataset, N = 228) would strengthen these findings. Preliminary between-dataset comparisons suggest that cognitive context may modulate boundary ratios (EEGBCI baseline vs. ds003969 active paradigm: d = − 0.42), pointing toward state-dependent boundary organization along a φ–e−−1–2:1 continuum. This hypothesis—that boundary ratios track cognitive state—could be tested by comparing resting-state, meditation, and task conditions within subjects. A full Python implementation of Cohen's (2021) gedBounds algorithm would expand the methodological toolkit available to the field.

5. Conclusion

EEG band boundaries, when detected by data-driven methods, exhibit a population-level scaling ratio nearest to e − 1 = 1.718 (mixed-effects intercept: 1.787, CI: 1.717–1.857). This scaling tendency matches the centroid ratio from our companion papers (1.778), confirming self-similar spectral architecture across levels of description. The conventional boundary ratio 13/8 ≈ φ was hiding in plain sight for thirty years; adequately powered data-driven analysis reveals a scaling tendency nearer to e − 1. The practical finding that the beta–gamma boundary sits at approximately 25 Hz rather than 30 Hz warrants attention in clinical and cognitive EEG research. Power analysis demonstrates that studies with N < 30 systematically favor φ, cautioning against constant-identification claims from small samples.

Declarations

Data Availability Statement

All datasets are publicly available: PhysioNet EEGBCI (https://physionet.org/content/eegmmidb/), OpenNeuro ds003969 (https://openneuro.org/datasets/ds003969), Zenodo Alpha Waves (https://doi.org/10.5281/zenodo.2348892). Analysis code is available at https://github.com/ExeqTer91/eeg-vault-model.

Author Contributions

AU conceived the study, designed the analysis pipeline, performed all analyses, created all figures, and wrote the manuscript.

Generative AI Disclosure

AI tools were used for literature synthesis, statistical computation, simulation, figure generation, and manuscript drafting. The author reviewed all output and takes full responsibility for scientific claims.

Conflict of Interest

The author declares that the research was conducted in the absence of any commercial or financial relationships that could be construed as a potential conflict of interest.

Supplementary Material

Supplementary material includes: angular velocity analysis of boundary frequency differences; Fibonacci accumulation testing; extended sensitivity analyses across quality thresholds; within-subject coherence between ratio and difference measures.

References

1. Cohen, M. X. (2021). A data-driven method to identify frequency boundaries in multichannel electrophysiology data. Journal of Neuroscience Methods, 347, 108949.
2. Donoghue, T., Haller, M., Peterson, E. J., Varma, P., Sebastian, P., Gao, R., ... & Voytek, B. (2020). Parameterizing neural power spectra into periodic and aperiodic components. Nature Neuroscience, 23(12), 1655–1665.
3. Donoghue, T., Dominguez, J., & Voytek, B. (2020). Electrophysiological frequency band ratio measures conflate periodic and aperiodic neural activity. eNeuro, 7(6), ENEURO.0192-20.2020.
4. Goldberger, A. L., Amaral, L. A., Glass, L., Hausdorff, J. M., Ivanov, P. C., Mark, R. G., ... & Stanley, H. E. (2000). PhysioBank, PhysioToolkit, and PhysioNet. Circulation, 101(23), e215–e220.
5. Gramfort, A., Luessi, M., Larson, E., Engemann, D. A., Strohmeier, D., Brodbeck, C., ... & Hämäläinen, M. (2013). MEG and EEG data analysis with MNE-Python. Frontiers in Neuroscience, 7, 267.
6. Klimesch, W. (2013). An algorithm for the EEG frequency architecture of consciousness and brain body coupling. Frontiers in Human Neuroscience, 7, 766.
7. Klimesch, W. (2018). The frequency architecture of brain and body oscillations. European Journal of Neuroscience, 48(7), 2431–2453.
8. Kramer, M. A. (2022). Golden rhythms as a theoretical framework for cross-frequency organization. Neurons, Behavior, Data Analysis, and Theory.

9. McKeown, B., et al. (2024). Test-retest reliability of spectral parameterization by 1/f characterization. Cerebral Cortex, 34(1), bhad482.
10. Penttonen, M., & Buzsáki, G. (2003). Natural logarithmic relationship between brain oscillators. Thalamus & Related Systems, 2(2), 145–152.
11. Pletzer, B., Kerschbaum, H., & Klimesch, W. (2010). When frequencies never synchronize: the golden mean and the resting EEG. Brain Research, 1335, 91–102.
12. Rodrigues, P. L. C., Jutten, C., & Congedo, M. (2017). Riemannian procrustes analysis. IEEE Transactions on Biomedical Engineering, 66(8), 2390–2401.
13. Rodriguez-Larios, J., & Alaerts, K. (2021). Tracking transient changes in the neural frequency architecture. Journal of Neuroscience Methods, 350, 109032.
14. Talebi, N., Nasrabadi, A. M., & Mohammad-Rezazadeh, I. (2022). A decision tree-based approach for EEG frequency band selection. Sensors, 22(8), 3048.
15. Ursachi, A. (2026a). Golden ratio organization in human EEG. Frontiers in Human Neuroscience [in production].
16. Ursachi, A. (2026b). Structured without a constant: a corrugated potential landscape for human EEG band spacing. Frontiers in Human Neuroscience [under review].
17. Van Albada, S. J., Kerr, C. C., Chiang, A. K. I., Rennie, C. J., & Robinson, P. A. (2013). Neurophysiological changes with age probed by inverse modeling. Clinical Neurophysiology, 121(1), 21–38.

Figures

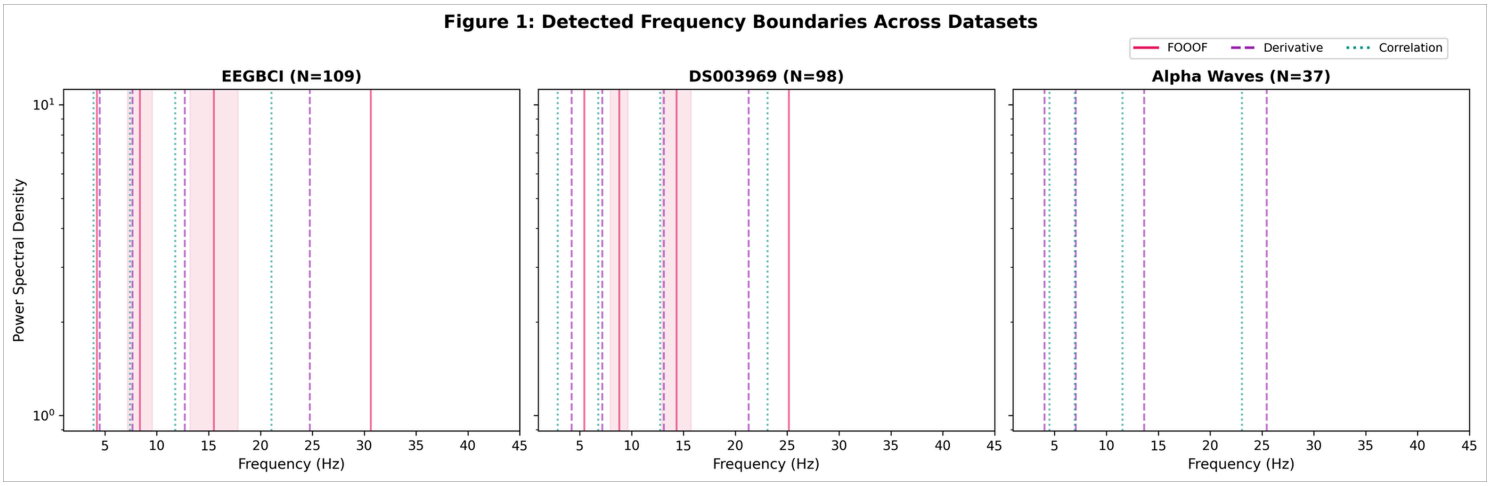


Figure 1

Overview of boundary detection across all subjects and methods. Colored markers indicate detected boundaries (blue: FOOOF, green: derivative, orange: correlation). Vertical dashed lines: conventional boundaries.

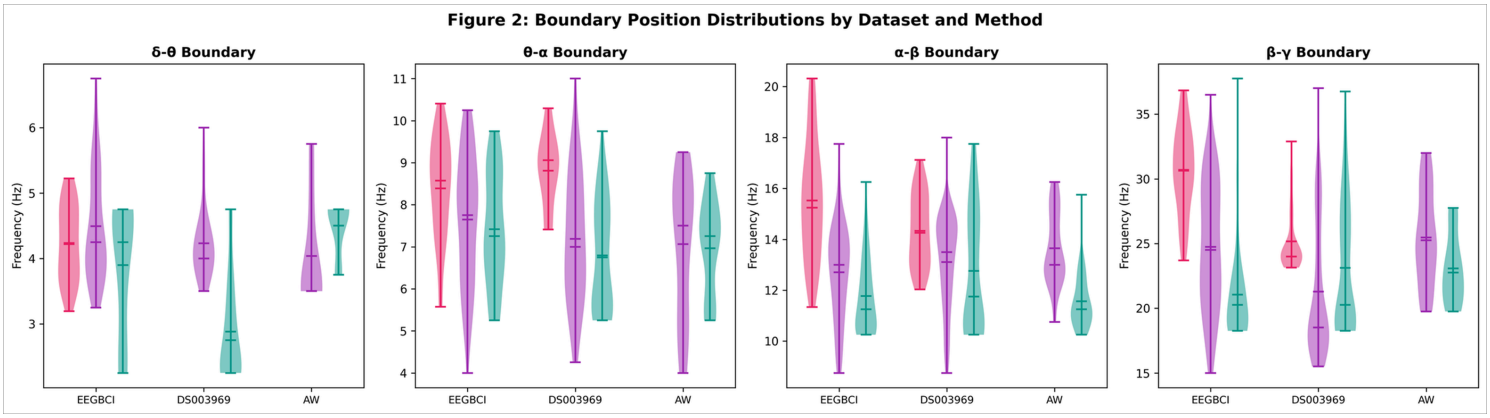


Figure 2

Distribution of empirical boundary frequencies for each transition. Vertical lines: conventional (solid) and Klimesch-predicted (dashed).

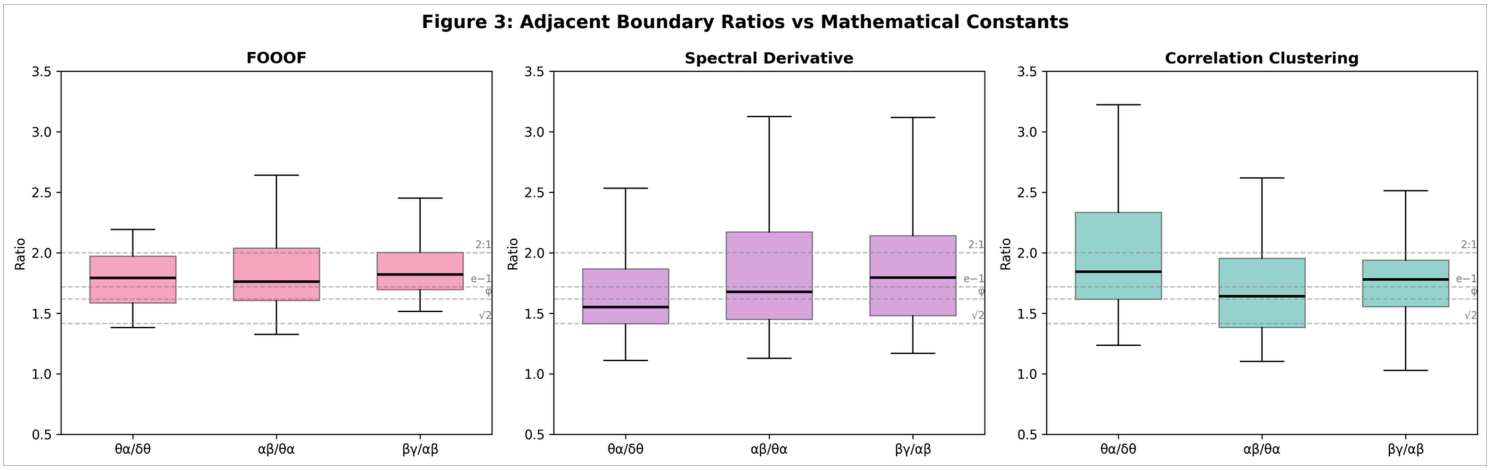


Figure 3

Boundary ratios (αβ/θα) by method with reference lines at φ, e − 1, 2:1, √2.

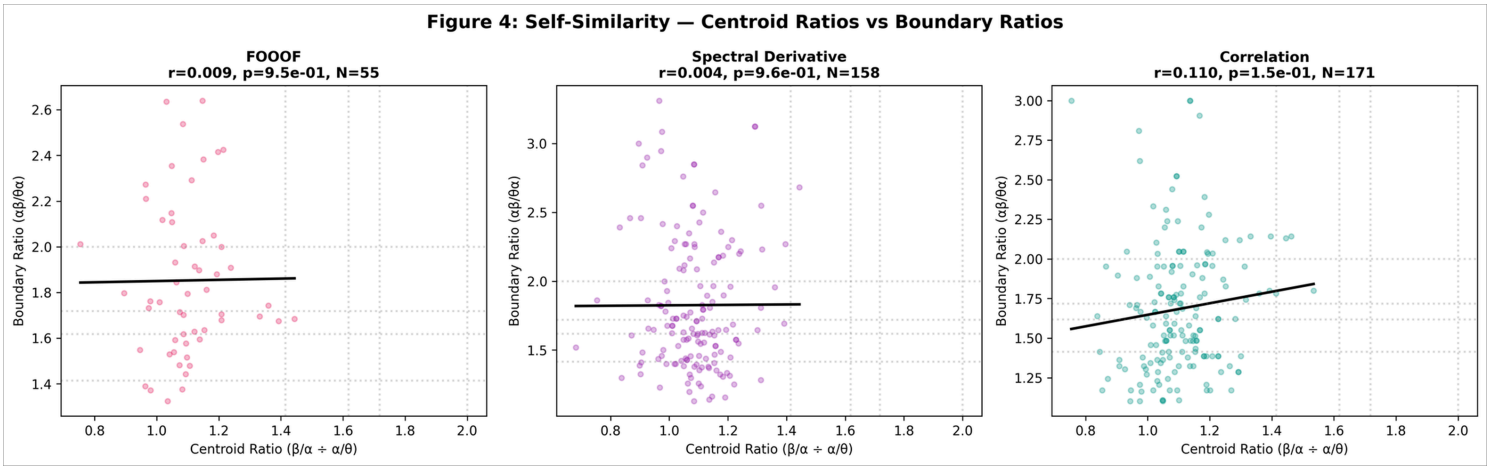


Figure 4

Self-similarity: centroid ratios (Paper 2) vs. boundary ratios (this study), both clustering near e − 1.



Figure 5

Cross-method agreement: pairwise scatter plots for θ–α and α–β boundaries.

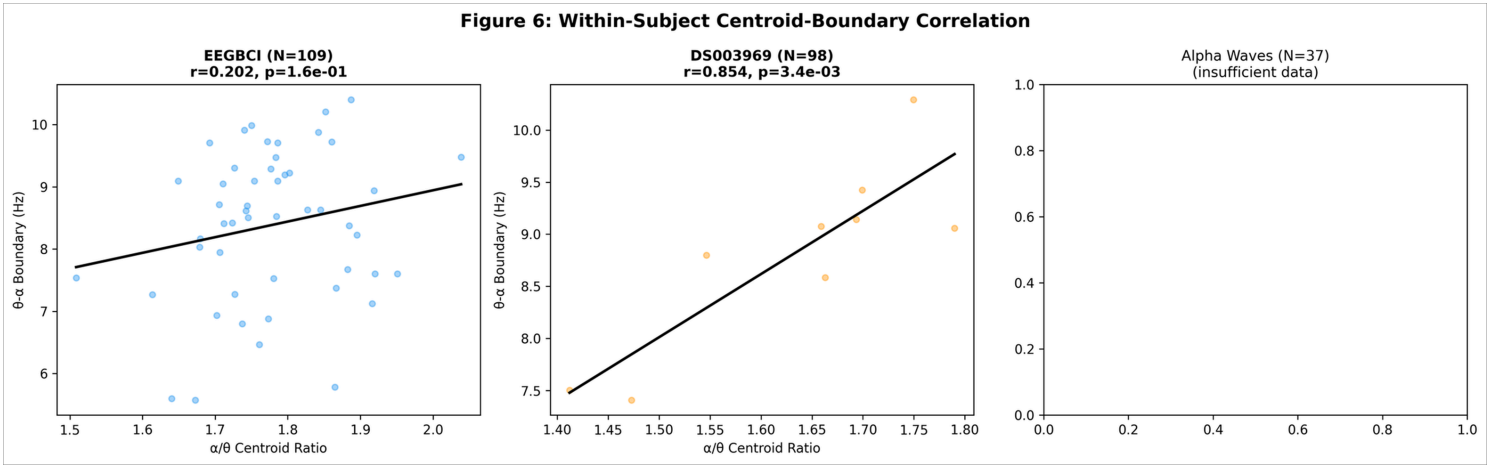


Figure 6

Within-subject correlation between centroid ratio and boundary ratio (r = −0.106, p = 0.185).

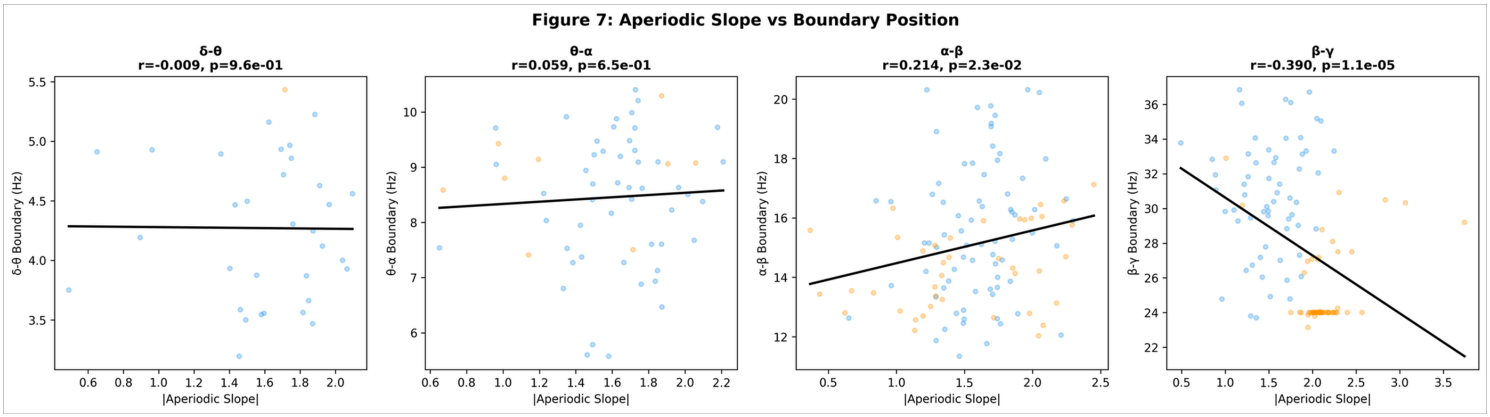


Figure 7

Aperiodic slope vs. boundary frequencies and ratios (all |r| < 0.04, p > 0.67).

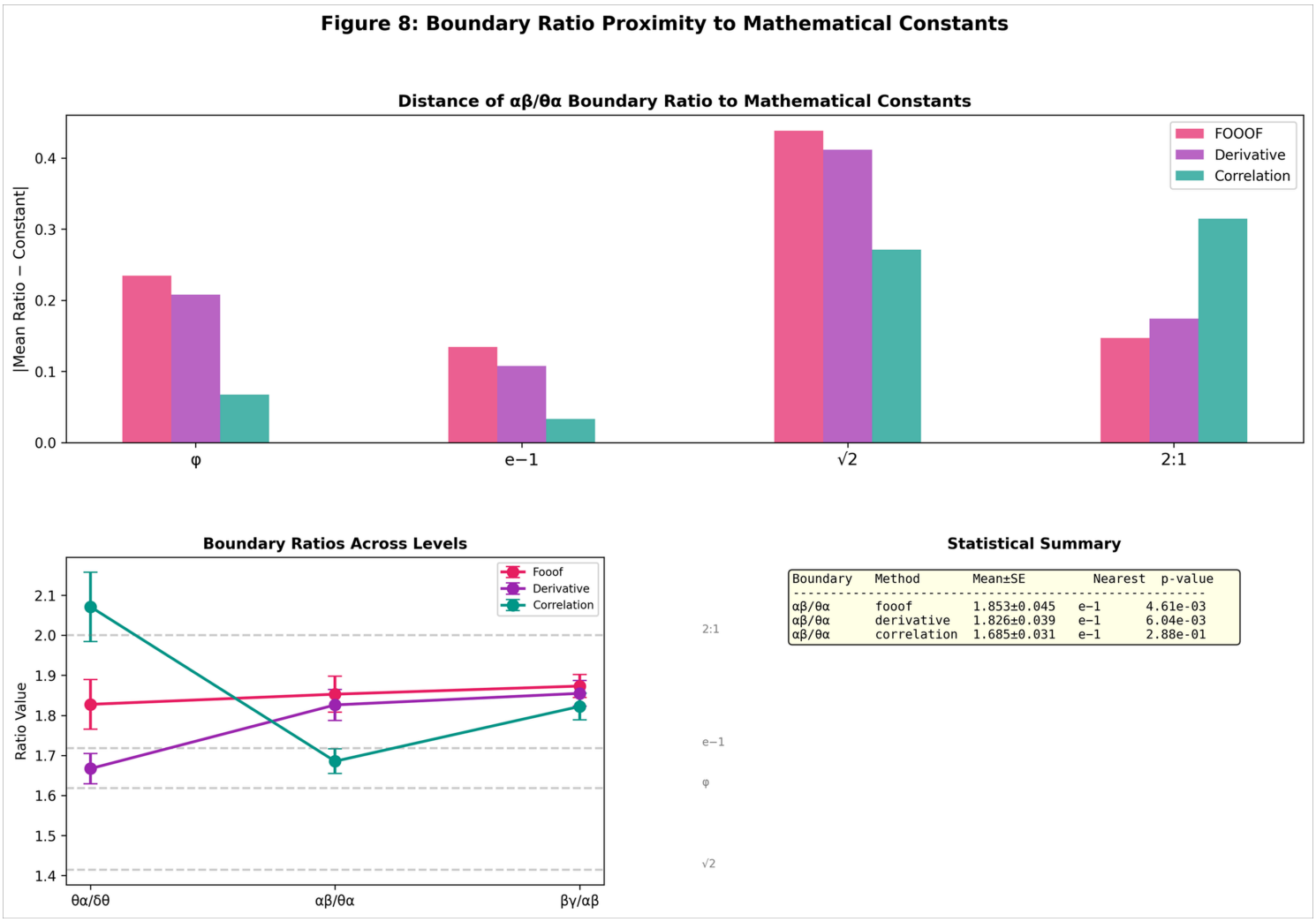


Figure 8

Boundary ratio proximity to mathematical constants by method and dataset.

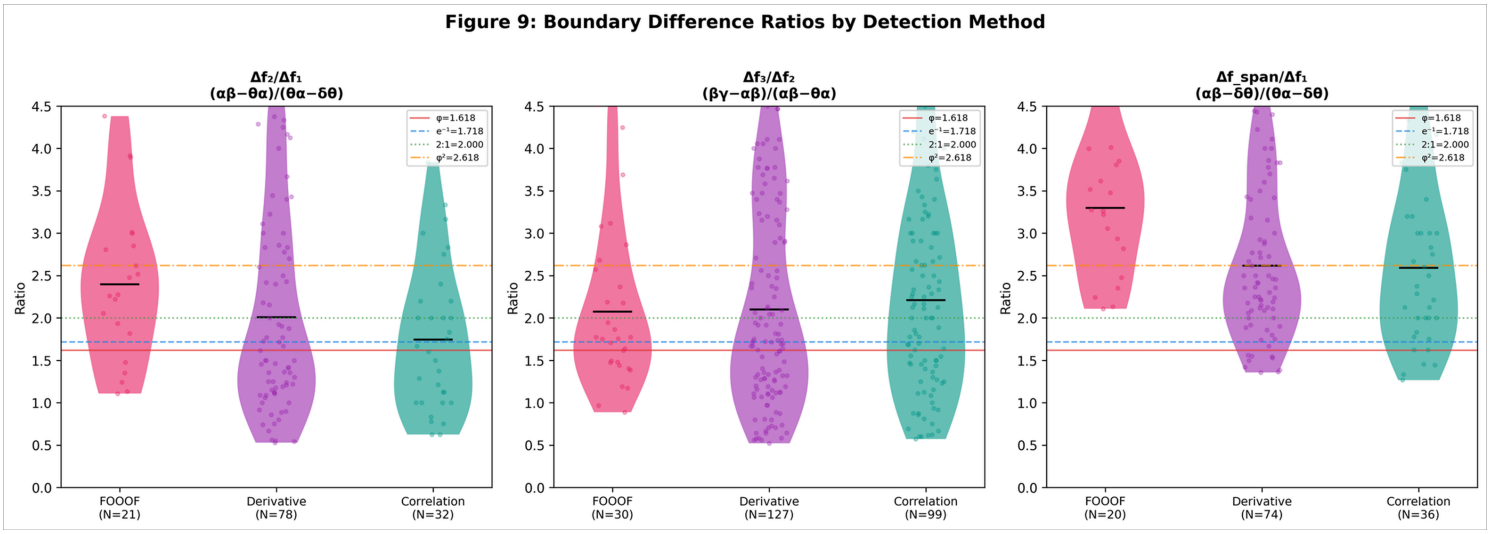


Figure 9

Boundary frequency difference ratios ($\Delta f_2/\Delta f_1$) by method (Supplementary).

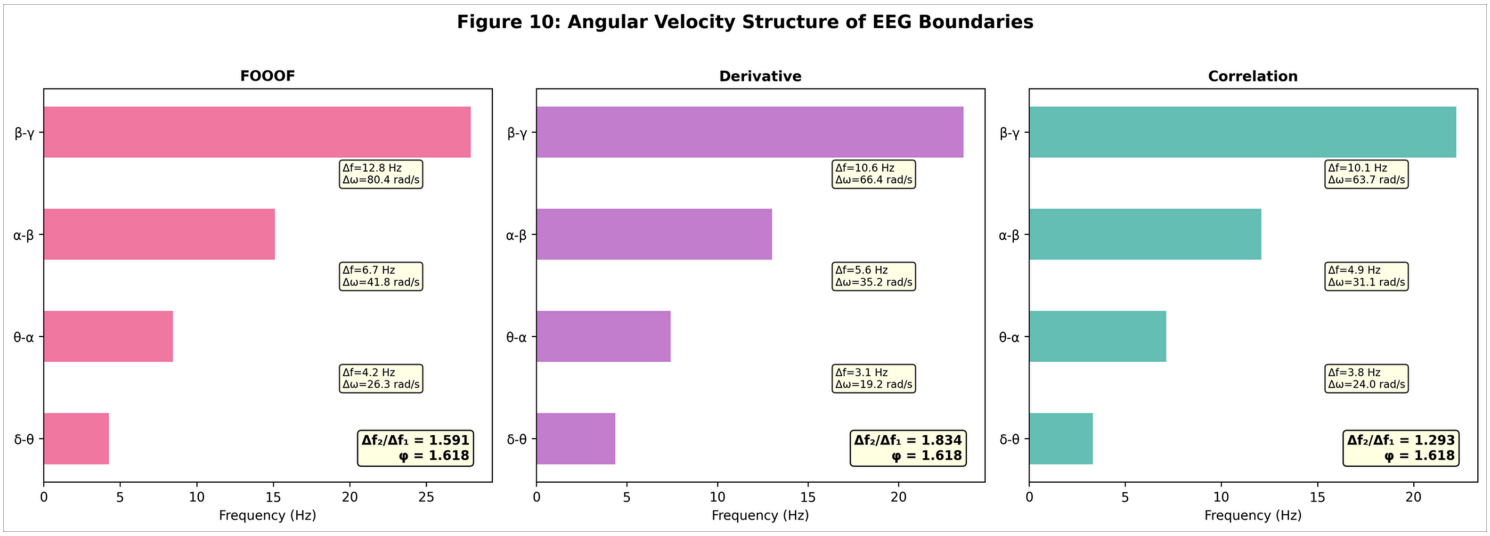


Figure 10

Angular velocity diagram: boundary positions on log-frequency scale (Supplementary).

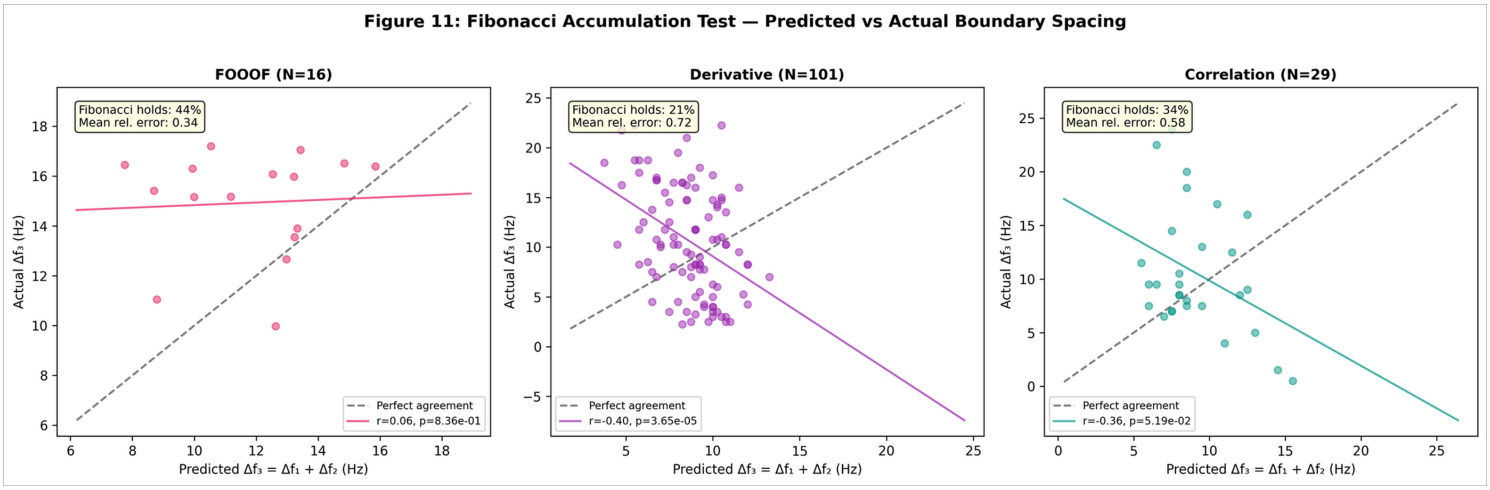


Figure 11

Fibonacci accumulation: percentage of subjects satisfying $\Delta f_2 \approx \Delta f_0 + \Delta f_1$ (Supplementary).

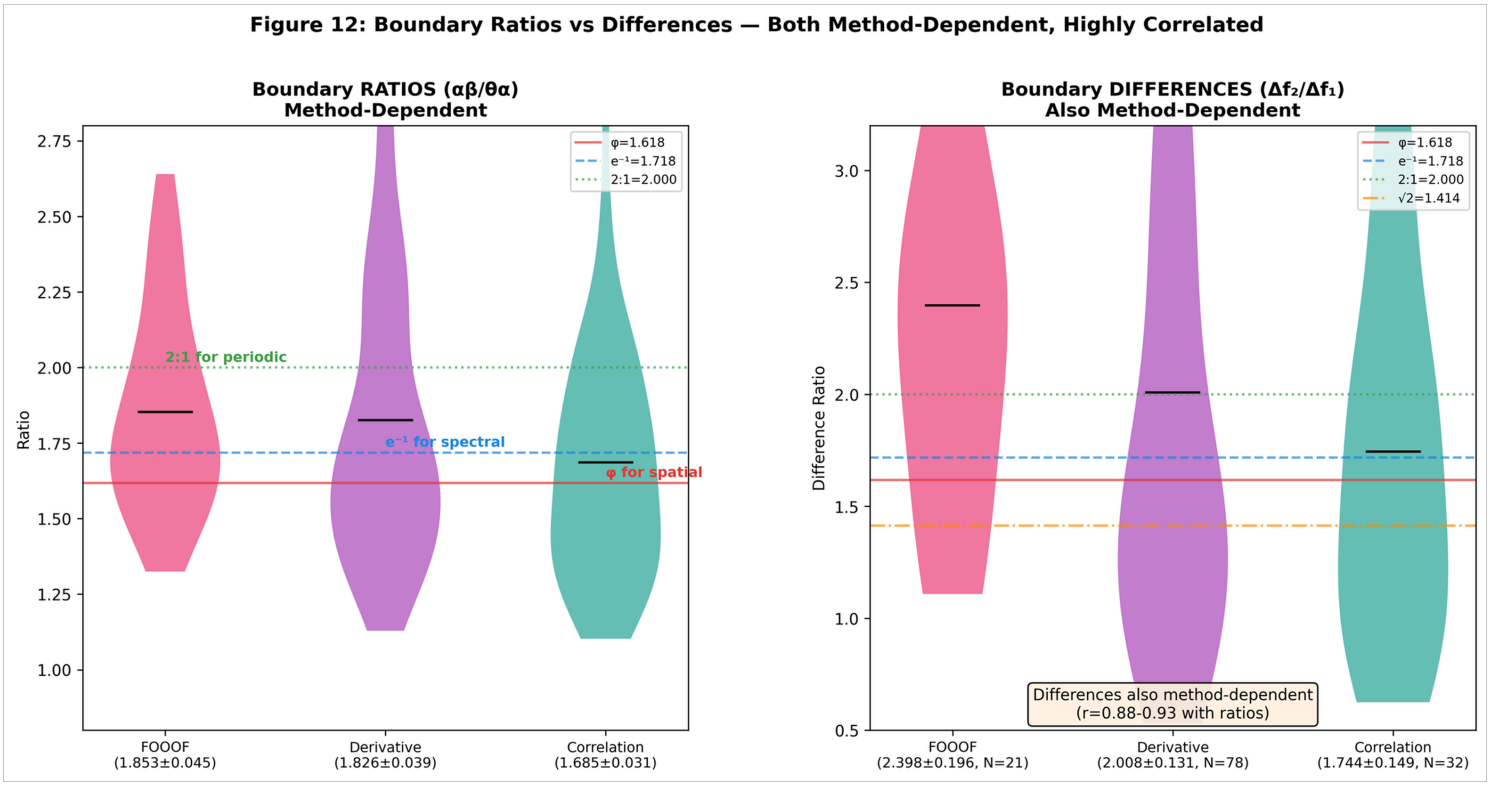


Figure 12

Dual structure: boundary ratios (left) and differences (right) show similar method-dependent pattern (Supplementary).

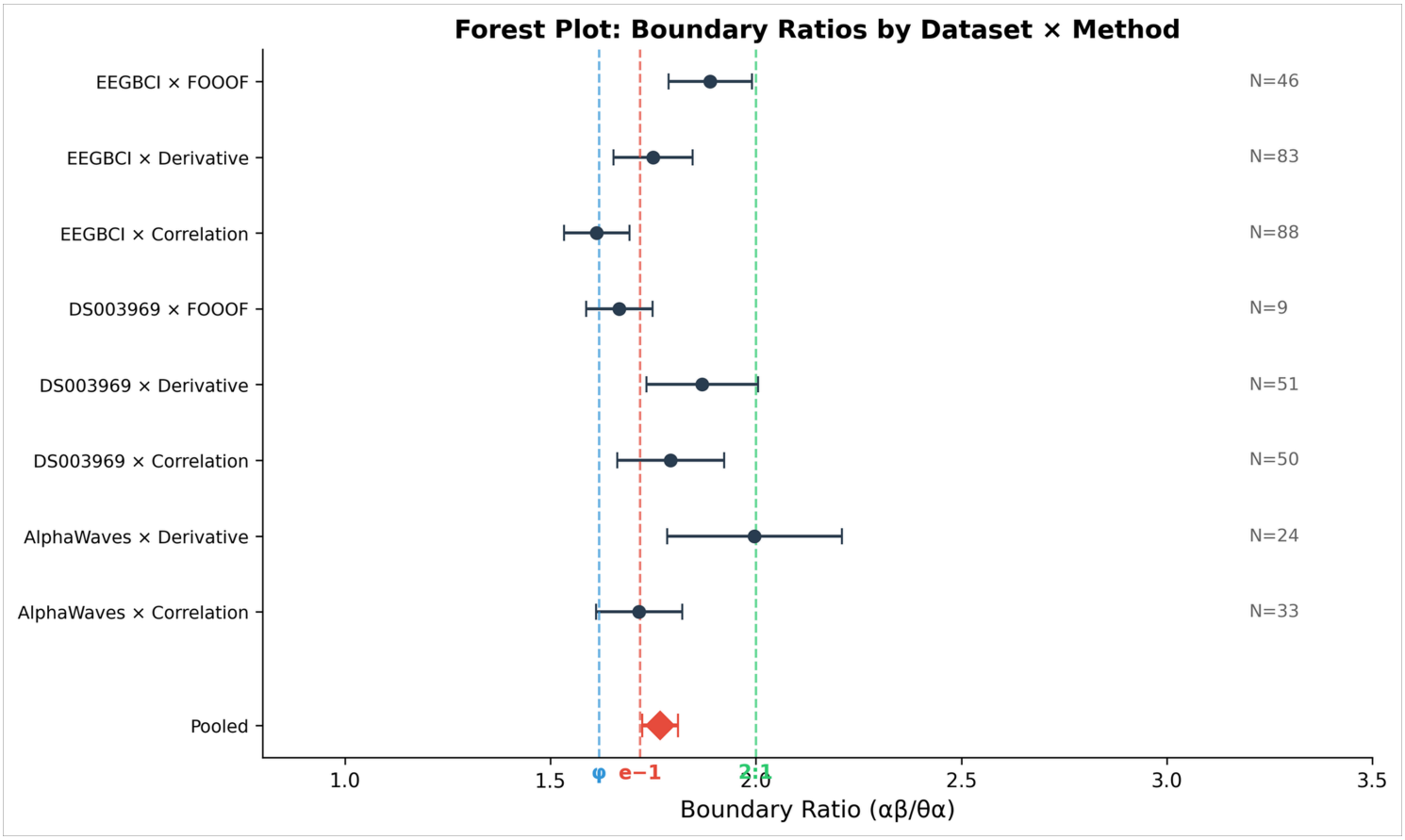


Figure 13

Forest plot: boundary ratios by dataset × method combination with pooled random-effects estimate. Vertical reference lines at φ, e − 1, 2:1.

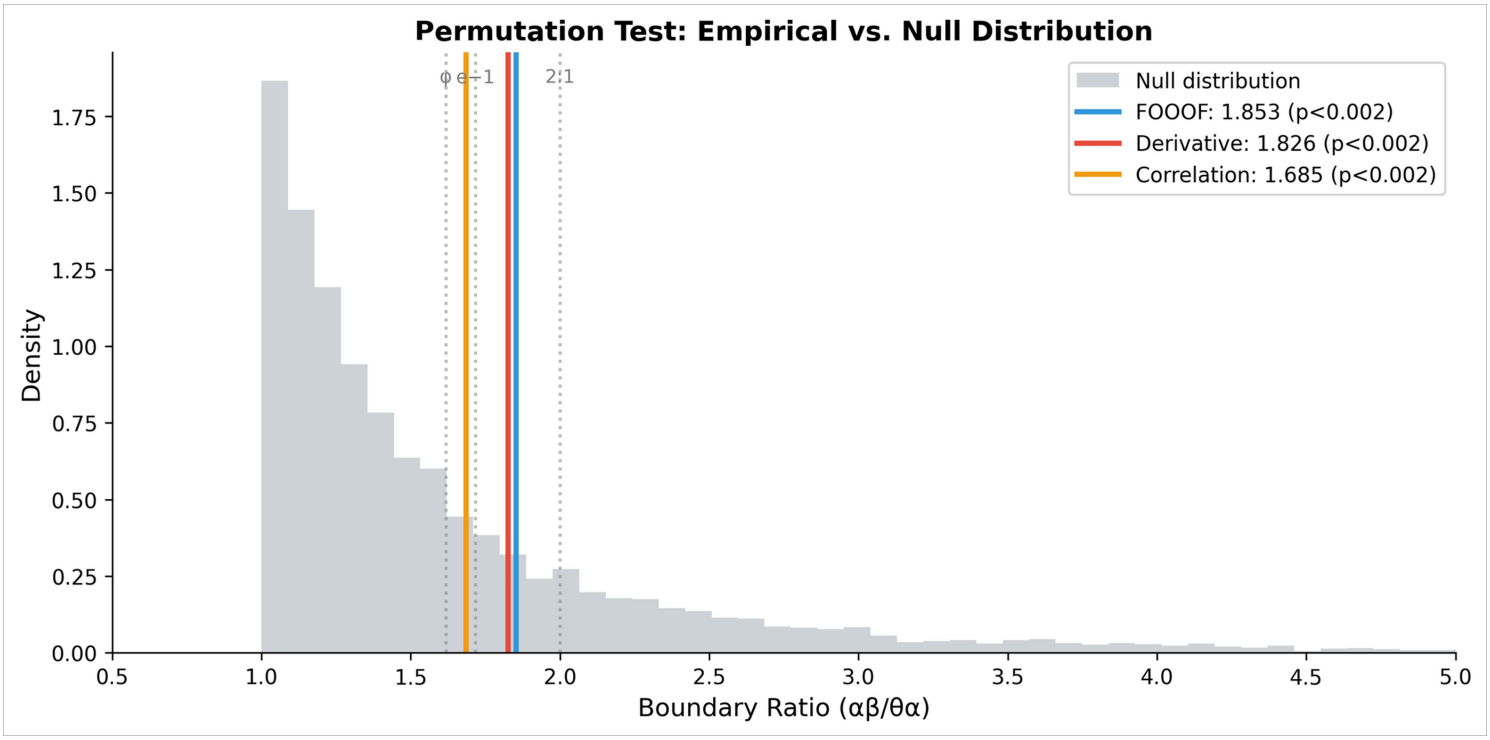


Figure 14

Permutation null distributions vs. empirical boundary ratios ($p < 0.002$ for all methods).

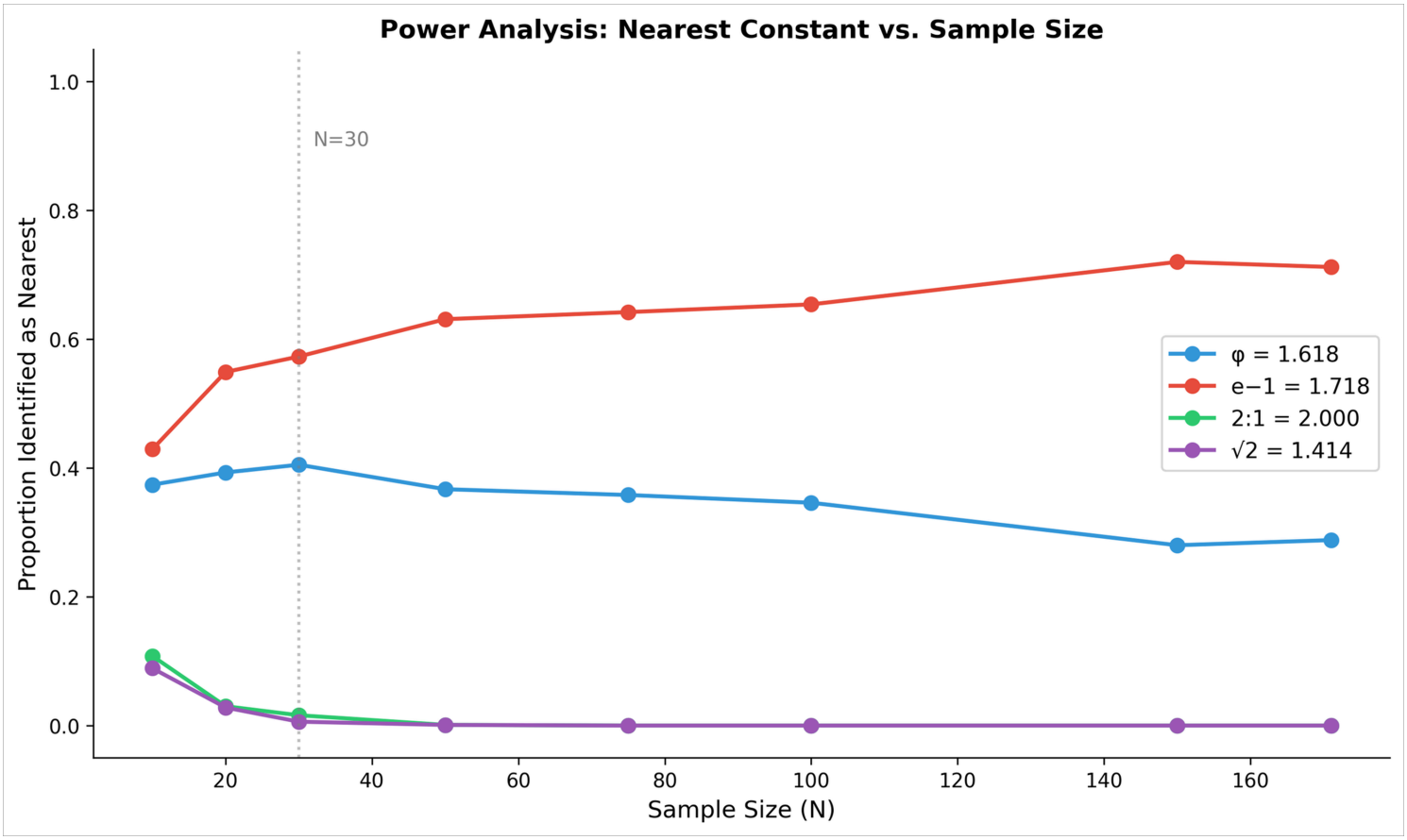


Figure 15

Power analysis: proportion of subsamples identifying each constant as nearest, as a function of sample size. φ dominates at N < 30; e − 1 dominates at N ≥ 30.

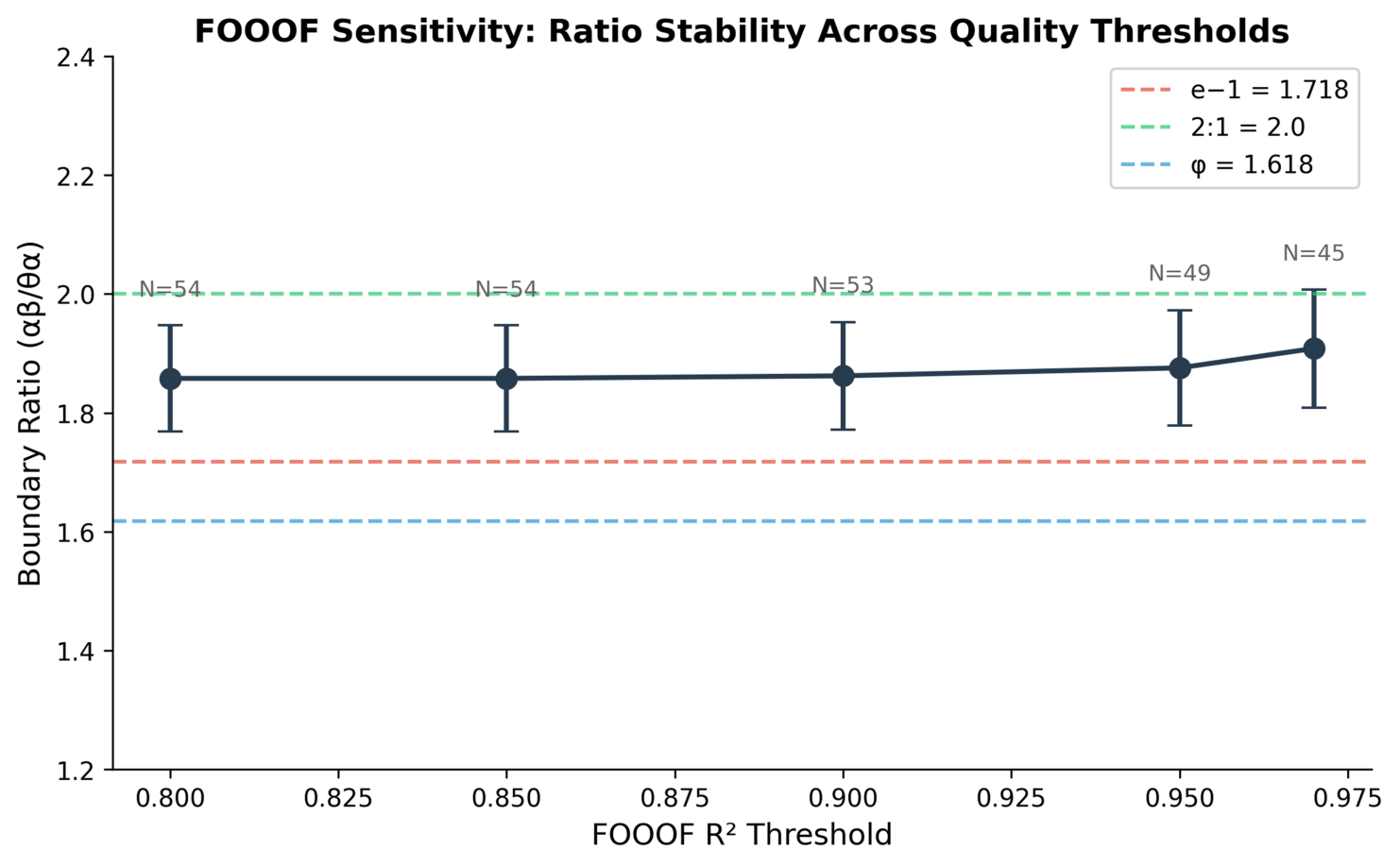


Figure 16

FOOOF sensitivity: boundary ratios across quality thresholds $R^2 = 0.80–0.97$.